nature neuroscience

On-going computation of whisking phase by mechanoreceptors

Avner Wallach[1,2], Knarik Bagdasarian[1] & Ehud Ahissar[1]

To attribute spatial meaning to sensory information, the state of the sensory organ must be represented in the nervous system. In the rodent's vibrissal system, the whisking-cycle phase has been identified as a key coordinate, and phase-based representation of touch has been reported in the somatosensory cortex. Where and how phase is extracted in the ascending afferent pathways remains unknown. Using a closed-loop interface in anesthetized rats, we found that whisking phase is already encoded in a frequency- and amplitude-invariant manner by primary vibrissal afferents. We found that, for naturally constrained whisking dynamics, such invariant phase coding could be obtained by tuning each receptor to a restricted kinematic subspace. Invariant phase coding was preserved in the brainstem, where paralemniscal neurons filtered out the slowly evolving offset, whereas lemniscal neurons preserved it. These results demonstrate accurate, perceptually relevant, mechanically based processing at the sensor level.

Sensory organs evolved intricate structures whose functional benefits are far from being understood. The complex follicles[1] of the long facial hairs of rodents (whiskers or vibrissae) are rhythmically moved when rodents scan and perceive their proximal surroundings[2–7]. To attribute spatial meaning to the tactually acquired sensory information, the current state of the sensory organ must be represented in the nervous system[8,9]. Previous studies have identified the on-going phase as a key coordinate and have reported phase-based representation of touch in the rodent's primary somatosensory cortex[4,10]. On-going phase, however, represents the whiskers' current position in an on-going cycle whose duration and amplitude are unknown a priori, and as such its extraction can be viewed as a predictive algorithm. Where and how such predictive computations are realized in the ascending afferent pathways remains unknown.

Vibrissal sensory information flows through the primary afferent cells of the trigeminal ganglion (TG). The peripheral endings of these pseudo-unipolar cells form mechanoreceptors in the follicle. The central processes of these cells project to the trigeminal sensory nuclei of the brainstem[1,11] (**Fig. 1a**). We studied the representation of whisker motion in the TG and brainstem by employing a closed-loop approach in anesthetized rats in which a real-time motion control algorithm substituted for the rat's internal control mechanisms (**Fig. 1b** and Online Methods). This algorithm consisted of a feedforward inverse model of the neuro-muscular system, working in parallel to a feedback controller that counteracts short- and long-term changes in the controlled system[12] (**Supplementary Fig. 1**). Using this technique, we were able to replicate behavior recorded in awake rats (**Fig. 1c** and **Supplementary Video 1**), as well as to generate long sequences of synthetic, behavioral-like movements (**Fig. 1d**); these consisted of rhythmic oscillations with phase φ ($-\pi \leq \varphi < \pi$; **Fig. 1e**), modulated by varying amplitude, offset (the midpoint angle of the oscillations), frequency (inverse of the duration of the cycle), and the ratio between protraction and retraction durations. Consistent with published behavioral data, whisking amplitude and offset were slowly modified between cycles[13], whereas whisking frequency was altered independently for each cycle[14] (**Supplementary Fig. 2**). The use of anesthetized rats enabled the application of well-controlled whisking patterns and the examination of the response of a large number of well-localized neurons to each specific pattern, so that the various input variables could be decoupled from one another. Moreover, this approach allowed us to explore the ascending afferent coding in the absence of top-down modulations. A total of 194 single units were recorded, of which the activity of 147 allowed reliable quantitative analysis.

RESULTS

Mechanoreceptors extract phase information from whisker motion

We first characterized the response properties of TG afferents to synthetic whisking trajectories, focusing on their responses to the three first-order kinematic variables (protraction angle, angular velocity and acceleration). Similarly to what was previously found using white-noise analysis[15], almost all of the recorded TG cells conveyed significant information on all three variables (Monte-Carlo $P < 0.05$, Online Methods; out of 47 cells, 39 responded to all three variables, 2 cells responded to angle and velocity, 3 cells responded to angle alone and 3 cells did not respond to any kinematic variable). In other words, most TG units responded preferentially to subregions of the kinematic space (**Fig. 2a**).

To reveal the input-output reduction in dimensionality exhibited by these units (often described as the units' input filters), we computed two projections in the multi-dimensional kinematic state-space that best describe the neuronal outputs that we recorded: the spike-triggered

[1]Department of Neurobiology, Weizmann Institute of Science, Rehovot, Israel. [2]Present address: Department of Cellular and Molecular Medicine, Faculty of Medicine, University of Ottawa, Ottawa, Ontario, Canada. Correspondence should be addressed to E.A. (ehud.ahissar@weizmann.ac.il).

Received 2 October 2015; accepted 4 December 2015; published online 18 January 2016; doi:10.1038/nn.4221

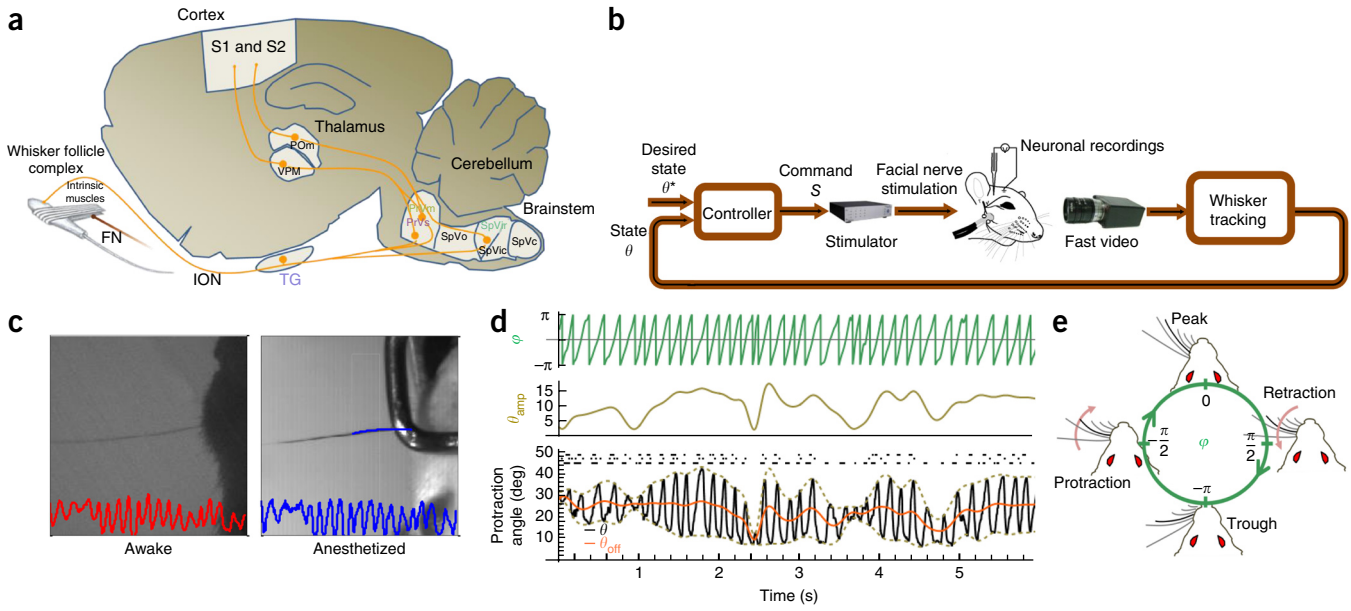

Figure 1 Closed-loop muscle-computer interface generates naturalistic whisking in anesthetized rats. (**a**) Vibrissal afferent pathways relevant to this study. ION, infra-orbital nerve; FN, facial motor nerve; PrV, trigeminal principal nucleus (which includes single-whisker PrVs cells and multi-whisker PrVm cells); S1 and S2, primary and secondary somatosensory cortices; subdivisions of trigeminal spinal nucleus: SpVo, oral; SpVir, rostral interpolar; SpVic, caudal interpolar; SpVc, caudal. Single-unit activity was recorded in the TG, SpVir and PrV. (**b**) Closed-loop stimulation set-up. Whisker motion was tracked online and a control algorithm altered motor-nerve stimulation in real-time to reproduce awake-like whisking trajectories (Online Methods). (**c**) Tracking of whisker protraction angle in an awake rat (left, red) and generation of the same trajectory in an anesthetized rat (right, blue) (**Supplementary Video 1**). To ease visual comparison, the movie chosen for this image is of a head-restrained rat. (**d**) Fast oscillations with phase φ (green, top) were modulated with slowly varying amplitude (θ_{amp}, gold, middle), and we added a low-frequency offset (θ_{off}, orange, bottom) to produce synthetic whisking sequences (θ, black, bottom). Raster in bottom panel: extracellular spikes concurrently detected in three SpVir single units. (**e**) Value of the phase φ at the different stages of the whisking cycle.

average (STA), a widely used projection that is related to the cross-correlation between the input (that is, whisker motion) and the units' activity, and the maximally informative dimensions (MID)[16], which describes the direction in input space yielding the highest mutual information with the cell's spiking activity. The input filters of TG neurons, as described by both these analyses, typically resembled the dynamics of a single whisking cycle, with different neurons firing preferentially at different times along this cycle (**Fig. 2a**). These projections suggest that the mechanoreceptors are predominantly tuned to the characteristic rhythmic motion of whisking. To analyze the rhythmic tuning of TG, we employed the rhythmic decomposition algorithm on the whisking dynamics[10]: after removal of the low-frequency offset component (θ_{off}, <4 Hz), amplitude and phase (θ_{amp} and φ) were extracted using the Hilbert transform. The resulting rhythmic state space clearly demonstrated preferential firing of TG neurons in specific phases in the whisking cycle (**Fig. 2a**). The units' preferred rhythmic phase closely matched the preferred STA and MID phases ($R^2 = 0.96$ for STA and $R^2 = 0.64$ for MID, $P < 10^{-3}$ for both, random permutations, $n = 41$; **Fig. 2b**). Overall, TG cells in our sample ($n = 41$ phase-informative cells) coded whisking phases across the entire whisking cycle, yet protraction was clearly over-represented (**Fig. 2b**). We conclude that mechanoreceptors at the whisker follicle appear to be tuned to fire at specific phases in the whisking cycle, consistent with previously reported indications[8].

These mechanoreceptors, however, are excited only by the mechanical forces exerted on the follicle during whisking, and the information generating the observed phase coding therefore exists entirely in the whisking mechanics, which in the case of whisker follicles is virtually fully reflected in whisking kinematics[17]. We note that extraction of ongoing phase from whisker mechanics is not a straightforward task: as a result of the variance in whisking amplitude, offset and frequency, any combination of angle and angular velocity (the first two dimensions of the kinematic space, hereafter referred to as the first-order kinematic state) corresponds to a range of phases (**Fig. 2c**) and vice-versa (**Fig. 2d**). Yet, phases are not distributed randomly in the kinematic space of naturally constrained whisking (**Fig. 2e**).

Reliability of TG preferred phase

Phase represents the relative state in a cycle and is determined in relation to the spatio-temporal trajectory of the whisker during the entire cycle (**Fig. 2d**). A reliable phase-coding cell would respond predominantly at the same 'preferred' phase, regardless of the cycle's amplitude or frequency. Given that the spikes are emitted before the cycle is completed, reliable phase coding requires prediction of both cycle duration (or its reciprocal, frequency) and amplitude on the basis of current and past kinematics.

We computed the phase tuning of TG units across the entire whisking frequency and amplitude ranges. The overall firing intensity of most cells was affected by both amplitude and frequency (43 and 38 units conveyed significant amplitude and frequency information, respectively). However, the preferred phase of most TG units was both frequency and amplitude invariant, with nearly vertical bands in the phase-frequency and phase-amplitude planes (**Fig. 3a**). Tuning invariance was quantified for each cell using the frequency- and amplitude-invariance indices (FII and AII), which measure the difference in preferred phase between high and low frequencies and amplitudes, respectively (**Fig. 3b**). For each cell, the significance of the frequency and amplitude dependence was estimated using a Monte-Carlo approach (Online Methods). The preferred phase of 73% and 66% of TG cells was not significantly modulated by frequency and amplitude, respectively ($P < 0.05$,

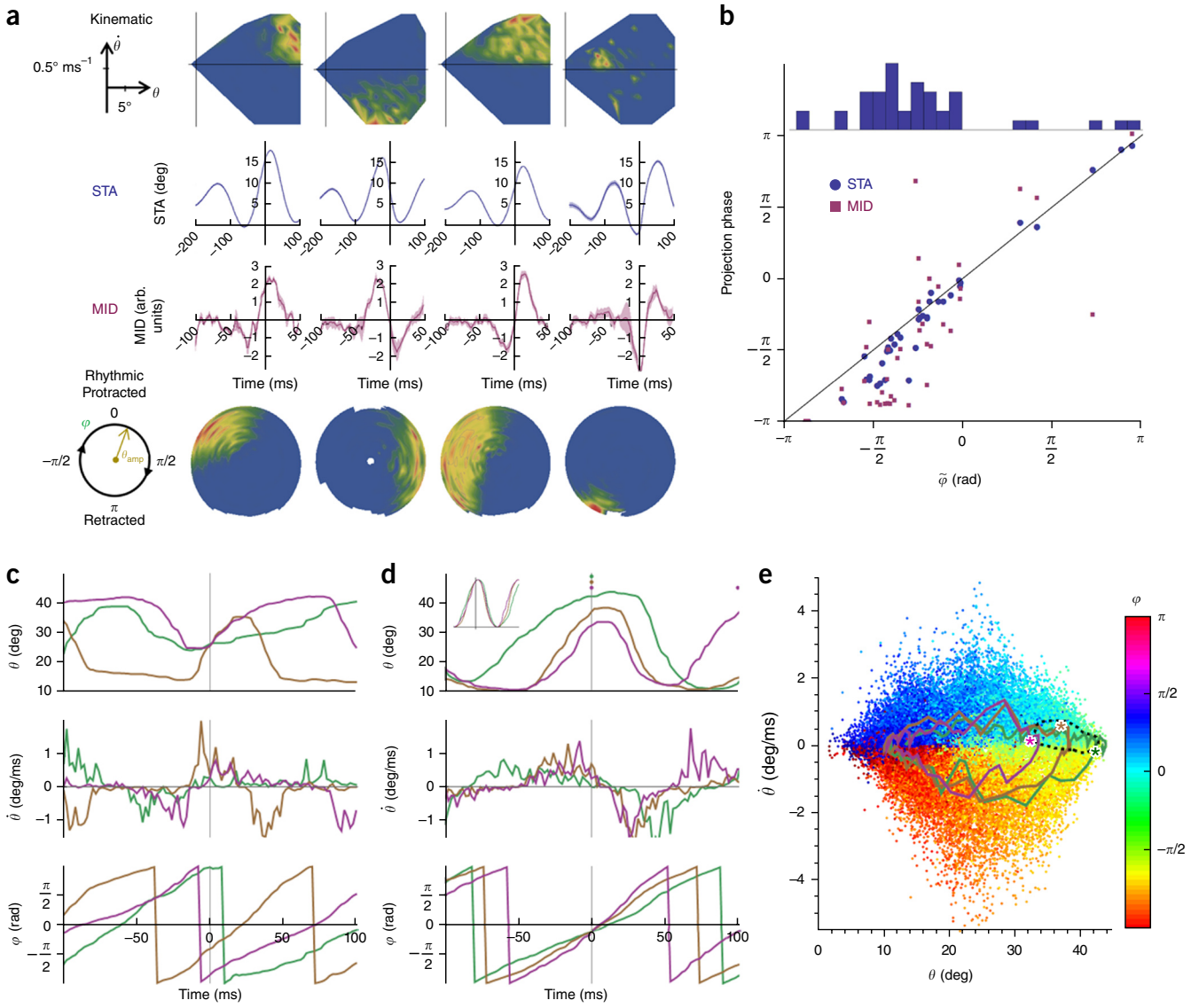

Figure 2 Representation of naturalistic whisker motion by follicle mechanoreceptors. (**a**) The response of four example TG single units to synthetic whisking dynamics (one unit in each column). Top, tuning surfaces to angle (θ) versus angular velocity ($\dot{\theta}$). Second and third rows, STA and MID projections for each unit. Bottom, phase versus amplitude tuning surfaces (presented in polar coordinates). (**b**) Input filter (STA and MID) preferred phase corresponded to the rhythmic response preferred phase $\tilde{\varphi}$, computed using the Hilbert transform. Top, distribution of preferred phases in TG. (**c**) Mapping from first-order kinematic state to phase was not unique; the three synthetic whisking trajectories shown have nearly identical protraction angle (top) and angular velocity (middle) at $t = 0$ (that is, they are tangential). However, the cycle phase at $t = 0$ (bottom) is very different in these three examples as a result of the variance in amplitude, offset and frequency. (**d**) Mapping from phase to first-order kinematics is non-unique; the three trajectories shown have nearly identical phase at $t = 0$ (bottom), but different kinematic state (angle and velocity, top and middle). A TG cell recorded in this session fired in all three instances at $t = 0$ (raster depicted in the top panel). Inset, the three angle trajectories after offset removal and normalization of both amplitude and frequency, demonstrating that the firing of the cell at $t = 0$ is equivalent to predicting the future evolution of the cycle. (**e**) Distribution of phases (color coded) in first-order kinematic space. Each dot is a single 2-ms sample. Superimposed: one cycle of each of the three trajectories of **c**, with the state in which a spike occurred in that cycle marked with an asterisk; dotted black line marks the kinematic region in which the cell responded throughout the experiment.

Monte-Carlo, Online Methods; $n = 41$, phase-informative TG cells; **Fig. 3c**). We note that whisking frequency was altered independently between cycles, so the cells could not adapt their response based on past cycle information. This invariant phase coding therefore had to be generated purely based on within-cycle past dynamics.

Kinematic model explains phase tuning frequency invariance

We attempted to explain TG cells' response with two types of models. First, we modeled each cell with a projection-based linear-nonlinear-Poisson (LNP) model, using a causal version of the MID filter of each unit as the linear filtering stage (Online Methods). Although the simulated models captured the general response properties (**Supplementary Fig. 3**) and amplitude invariance of most of the phase informative cells (61%, $n = 41$), they exhibited frequency invariance for only less than half of the phase informative cells (44%, $n = 41$ cells; **Fig. 3a**,**c**).

We next asked whether invariant phase tuning can be obtained from the information contained in the first-order kinematic state.

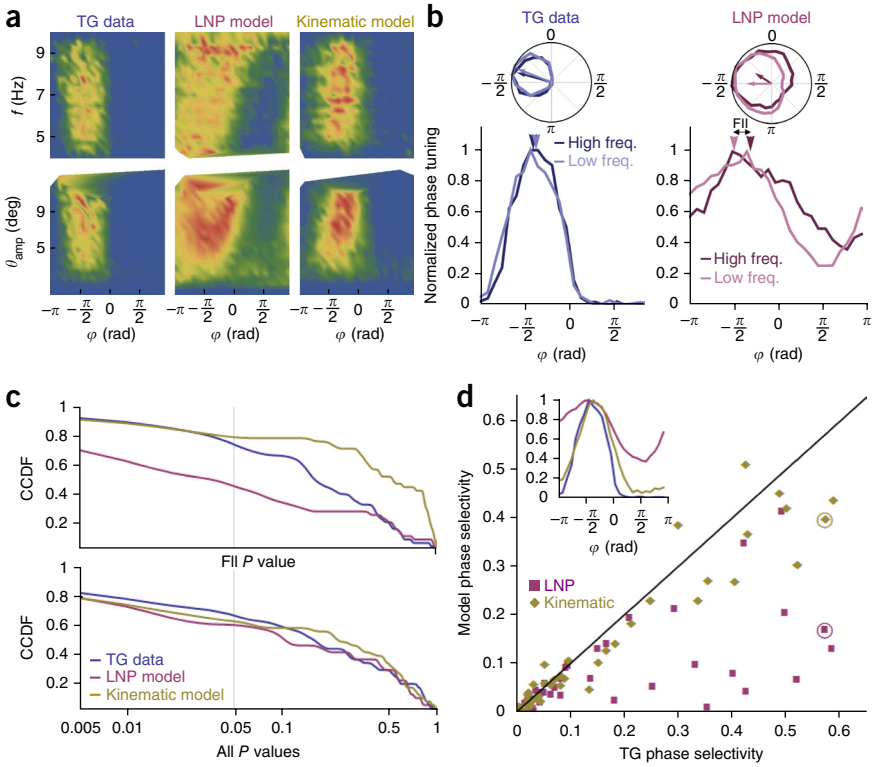

Figure 3 Invariance coding and modeling. (**a**) Phase tuning of a TG unit (left), its LNP model (middle) and its kinematic model (right) across the range of whisking frequencies (top) and amplitudes (bottom); the more vertical the bands are the more invariant phase tuning is. (**b**) FII calculation for the cell in **a** and for its LNP model. Phase tunings (normalized to the maximum) for high and low frequencies (dark and light colored, respectively) are depicted in Cartesian (bottom) and polar (top) coordinates. Complex plane summation was used to obtain the phase vector of each tuning curve (arrows), the angle of which is the preferred phase (arrowheads). The difference between the two preferred phases (in radians) is the FII (the same procedure was applied for amplitude invariance). (**c**) Significance of preferred phase dependence on frequency (top) and amplitude (bottom) for TG units (blue), their LNP models (purple) and their kinematic models (yellow). The distributions of *P* values are plotted using the complementary cumulative distribution (CCDF, survival function); note the logarithmic scale. (**d**) Phase selectivity of TG units and their models. Inset, normalized phase tuning of the TG unit depicted in **a** and of its models. The selectivity values corresponding to this cell are circled.

Each kinematic tuning surface (**Fig. 2a**) was fitted with a bivariate Gaussian, which was then used to determine the instantaneous firing rate of a simulated non-homogenous Poisson process (Online Methods and **Supplementary Fig. 3**). These kinematic models generate frequency- and amplitude-invariant preferred phases in 78 and 63% of the cases, similar to what was observed in TG cells (n = 41; **Fig. 3a**,**c**). Non-parametric interpolation of the kinematic tuning, applied instead of surface fitting, yielded similar results (data not shown), indicating that the precise shape of the two-dimensional surface is not essential to this phenomenon. In contrast, we found that responding in a restricted

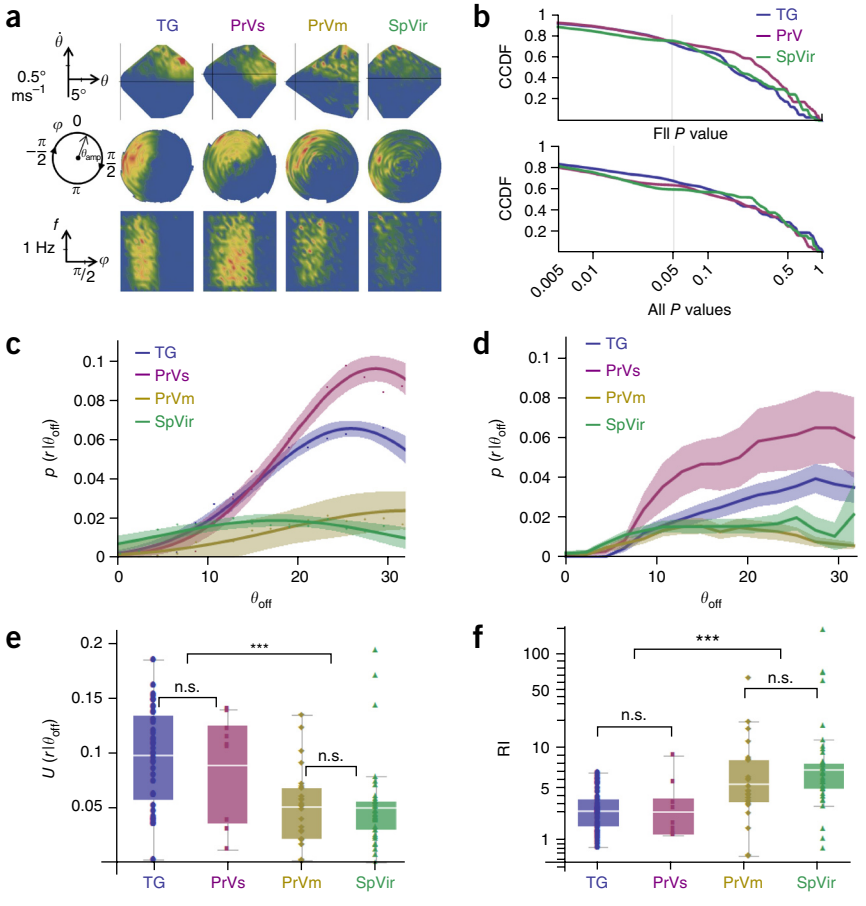

Figure 4 Representation of naturalistic whisker motion in the brainstem. (**a**) The response of four example units to synthetic whisking dynamics, one cell from each population sampled (columns). Top, angle versus angular-velocity analysis; Middle: phase versus amplitude analysis; Bottom: phase versus frequency analysis (vertical bands imply invariance). (**b**) Significance of preferred phase dependence on frequency (top) and amplitude (bottom). The distributions of *P* values are plotted using the CCDF; note the logarithmic scale. (**c**) Protraction offset (θ_{off}) tuning of the four units presented in **a**, fitted with Gaussians (shaded areas show 95% confidence interval). (**d**) Mean offset tuning curves for all four populations (shaded areas depict s.d.). (**e**) Distributions of the protraction offset information content (normalized mutual information, Online Methods) in the neuronal responses of each population. (**f**) Rhythmicity index (rhythmic/non-rhythmic information ratio, Online Methods) distributions for each population (note the logarithmic scale).

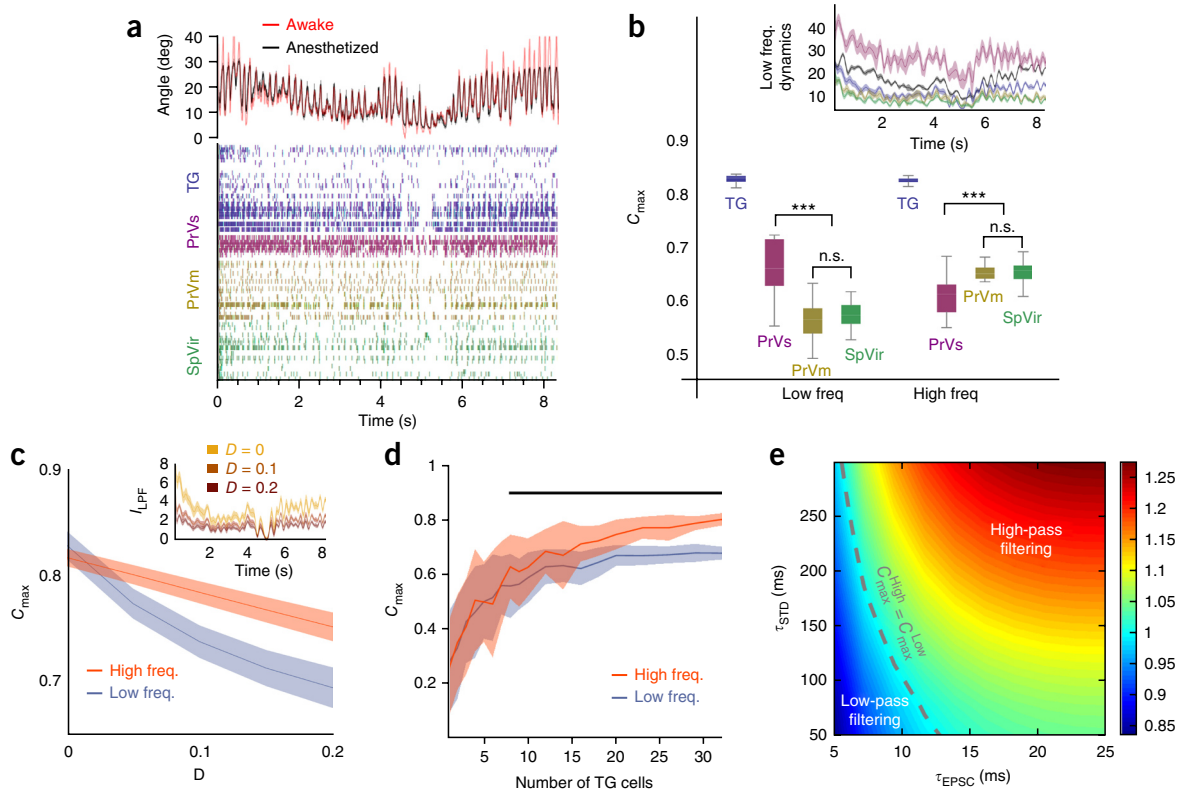

Figure 5 Early information processing in whisking-related afferent pathways. (**a**) Top, a single-whisker trajectory taken from a freely moving awake rat (red) was replayed 17 times for each unit recorded. The whisker motion obtained using closed-loop stimulation in anesthetized rats is plotted in black (mean in solid line, shaded area is s.d.). Bottom, spike raster of all whisking-sensitive units for the tenth repetition of the trajectory ($n = 102$ cells). (**b**) Peak correlation (C_{max}) distributions in the low- and high-frequency bands for all populations. Inset, low-frequency whisking dynamics (θ_{off}, deg, black) and low-frequency firing rate dynamics (r_{LPF}, Hz/unit) in all populations (Online Methods). (**c**) High-pass filtering reproduced by classic STD model. Peak correlation (C_{max}) between whisking dynamics and simulated membrane current in the low- and high-frequency bands (blue and red, respectively, mean ± s.d.), for varying degrees of STD. Inset, low-frequency membrane current dynamics for different STD levels. (**d**) C_{max} in the high- and low-frequency bands as a function of presynaptic population size (mean ± s.d.). Significant difference between the correlations was obtained for eight afferents or more (thick black line, $P < 0.041$, bootstrap, 17 repetitions). $D = 0.2$. (**e**) Ratio between high and low peak correlations ($C^{high}_{max} / C^{low}_{max}$) for different simulation parameter values ($D = 0.2$, entire TG population used).

kinematic subregion (for example, dotted black contour in **Fig. 2e**) is crucial for invariant phase tuning, as expanding the region destroys tuning invariance and selectivity (data not shown). These analyses show that the ability of TG cells to perform the predictive computation needed for reliable phase coding depends on the distribution of phases in the kinematic space, which in turn is dictated from the constraints that natural whisking kinematics adhere to. A conjecture of this is that phase coding reliability should deteriorate as the kinematics depart from these natural constraints, as was observed when open-loop square wave patterns were used (**Supplementary Fig. 4**).

We next tested how well the models capture the phase selectivity of the mechanoreceptors by comparing the width and steepness of their phase tuning with that of their simulated model. Both models' phase tuning was significantly broader than that of the cells ($P < 10^{-3}$, Wilcoxon signed-rank test for the difference between TG and model selectivity, $n = 41$; **Fig. 3d**). This inferior selectivity of the kinematic model is not a result of the fitting procedure employed, as this inferiority persisted when phase tunings in individual loci in the kinematic space were compared (**Supplementary Fig. 5**). This indicates that, although the two-dimensional kinematic model suffices in explaining the frequency and amplitude invariance of the phase response, it falls short of explaining the sharp phase selectivity of TG afferents.

Differential information processing in the brainstem

Whisking phase information is a predominant aspect of thalamocortical processing of object location[10,18]. Our results suggest that thalamocortical phase coding can be inherited from the mechanoreceptors rather than computed by down-stream neural circuits. We examined the transformations of TG phase coding at the intermediate processing station, the brainstem's trigeminal complex (**Fig. 1a** and **Supplementary Fig. 6**). We focused on the two trigeminal nuclei previously linked with processing whisker self-motion[19]: the principal nucleus (PrV), which contains two distinct populations, single-whisker cells (PrVs) and multi-whisker cells (PrVm); and the rostral part of the spinal interpolar nucleus (SpVir). Repeating the experiments and analyses in these structures yielded results very similar to those found in TG (**Fig. 4a**,**b**). Protraction phases were over-represented in all regions ($P < 10^{-3}$, Pearson's chi-square test, $n = 41$, 42 and 47 phase informative cells in TG, PrV and SpVir, respectively), with the majority of responses being concentrated in the second half of the protraction period ($[-\pi/2\ 0]$). 73, 76 and 74% of TG, PrV and SpVir were frequency invariant, and 66, 60 and 63% were amplitude invariant, respectively ($n = 41$, 42 and 47). Thus, it appears that the brainstem populations inherit the rhythmic phase representation generated by the follicle mechanoreceptors.

Comparing the representation of whisking dynamics in the different populations requires examining slow as well as fast components of the dynamics. To this end, we next considered the slow changes in the angle around which these oscillations are made (whisking offset θ_{off}; **Fig. 1d**). We observed a substantial difference in the representation of this low-frequency (<4 Hz) component of the whisking dynamics; although TG and PrVs units were highly sensitive to it, PrVm and SpVir cells were only weakly responsive to this variable. This is manifested in the tuning curves of both individual cells (**Fig. 4c**) and of the entire populations (**Fig. 4d**). This difference is reflected in the information content of the different units, with units in TG and PrVs conveying on average about twice as much information about the offset as units in PrVm or SpVir ($P < 10^{-3}$, bootstrap, $n = 52$ and 67 offset-informative cells, respectively; **Fig. 4e**). As a consequence, PrVm and SpVir are more 'rhythmic', in the sense that most of the information they convey is related to the high-frequency rhythmic components of whisking ($P < 10^{-3}$, bootstrap, $n = 52$ and 67; **Fig. 4f**). Thus, although both high- and low-frequency information is passed down to the single-whisker cells of PrV, a filtered version is conveyed to the multi-whisker cells of PrV and the SpVir nucleus, limiting their focus to the fast rhythmic components of whisking. Such attenuation of the low-frequency components is referred to in the engineering literature as high-pass filtering.

To test whether phase coding and its differential down-stream processing hold for natural-like whisking patterns, we recorded the responses of all our recorded units to repeated presentations of one characteristic motion recorded in a freely moving awake rat ('awake-playback' protocol, Online Methods; phase coding was preserved under this stimulation procedure in all units; **Supplementary Fig. 4d**). This systematic presentation of the exact same pattern to all our units enabled the reconstruction of the populations' responses to this motion (**Fig. 5a**). Brainstem populations' firing rate dynamics exhibited the same differential filtering observed in single units; although all three brainstem populations were less correlated with whisking than the TG population, the PrVs population was relatively more correlated in the low-frequency band and the PrVm and SpVir populations were more correlated in the high-frequency band ($P < 10^{-3}$, bootstrap, $n = 17$ repetitions; **Fig. 5b**).

Synaptic dynamics can explain differential brainstem processing

Differential processing of afferent information in the brainstem could be based on differential short-term dynamics of afferent synapses. A recent study found classic short-term depression (STD) dynamics in the afferent input to SpVir, as well as in the input from adjacent (non-principal) whiskers to PrVm; in contrast, the principal whisker input to PrV (and therefore the only input to PrVs cells) displayed anomalous depression profiles[20] (**Supplementary Fig. 7**). To test whether synaptic dynamics can explain our brainstem data, we simulated the effects of synaptic STD on our TG firing data (Online Methods). Indeed, the simulation revealed that increasing STD decreases the transmission of low-frequency modulations more than the transmission of high-frequency modulations, effectively generating a high-pass filter (**Fig. 5c**). Another factor that might be involved is the difference in presynaptic population size; although PrVm and SpVir are driven by many TG afferents, PrVs units are driven by only a few. Our simulation suggests that high-pass filtering requires input from several TG units (**Fig. 5d**). The high-pass filtering result held in a wide range of simulation parameters (**Fig. 5e**). The anomalous depression dynamics of the TG to PrVs synapses[20] were not included in this simulation. We speculate that these anomalous dynamics, which may be attributed to the inhibitory connections from SpVir[21] (**Supplementary Fig. 7**), help local PrV circuitry[22] in balancing low- and high-frequency responses of PrVs neurons. We conclude that the differences in afferent synaptic ensembles driving the brainstem populations are sufficient to explain the differential information processing exhibited in these populations.

DISCUSSION

Our most surprising finding is the ability of mechanoreceptive afferents to represent whisking phases in a reliable and selective manner; we found that most of these cells and their brainstem targets tended to fire at specific phases in the whisking cycle, irrespective of the cycle's amplitude or duration. As this invariant phase computation is performed while the cycle is on-going, mechanoreceptor coding can be viewed as being equivalent to predicting the future evolution of the whisking cycle. The relative success of the first-order kinematic model in reproducing frequency- and amplitude-invariant phase tuning demonstrates that this capacity relies on the constrained dynamics of natural whisking and requires the cells to respond in a restricted region in the angle-velocity kinematic space. Notably, a recent study found array of club-like mechanoreceptors in the follicular ringwurst structure that surrounds the vibrissal shaft[11], which, together with the rotation of the follicles during protraction[23], may enable the kinematic-to-phase transformation along the whisking cycle[8].

As we found, however, the high selectivity to phase exhibited by TG units were not fully reproduced by the first two kinematic variables. One possibility, which we were unable to test as a result of the unrealistic amount of data required for it, is that higher kinematic dimensions (angular acceleration, jerk) would add the missing information. Another possibility is that the dynamics related to the specific structure of specialized receptors, such as the ringwurst club-like receptors[11], contain the missing information. And finally, adaptive input-output dynamics such as gain rescaling[24] might take part in fine-tuning the phase response.

The significance of the invariant phase coding that we observed depends on if and how it may contribute to perceptual processes. It is important to emphasize that, although the preferred phase of a majority of the cells was independent of frequency and amplitude, the overall firing rate was not. This means that for any given cell a certain response rate may correspond to multiple phases, depending on the current amplitude and frequency (as well as offset, in the cells responding to it). Explicit decoding of phase from the spike rate may therefore necessitate concurrent decoding of amplitude and frequency (for example, by using different spike statistics[25]) or triangulation of responses across different neurons with similar preferred phase. Such schemes obviously gain little from the invariance we observed. Decoding schemes that focus on individual spikes, however, may exploit this feature in a rather straightforward way. We note that the best estimation of cycle phase, given a spike from a phase-sensitive cell, is the preferred phase of that cell[26]. A neuron receiving inputs both from such a phase-sensitive cell and from a 'touch' cell (that is, cell responding only to whisker-object contact) can be tuned to fire preferentially when an object is contacted at the preferred phases[8], regardless of the current whisking frequency or amplitude. Such downstream neurons need not be hypothesized, as cells with this exact behavior were already reported in the main cortical target of vibrissal afferent information, the primary vibrissal somatosensory cortex[10]. This type of neuronal activity may have a crucial role in the learning and execution of object localization[27,28].

The phase information extracted from the kinematics, along with information on amplitude, offset and frequency, is conveyed to the different brainstem recipient nuclei where it is further processed. Apart from the ascending afferent activity from the follicle

mechanoreceptors, the brainstem's trigeminal complex receives descending input from various brain regions[29–31]. We used anesthetized rats, with the motion being generated peripherally using our closed-loop control algorithm, presumably eliminating any motor-related efferent inputs. Thus, the brainstem responses we observed should be taken as primarily describing the ascending afferent input into the brainstem in the absence of top-down modulation. We found that single-whisker cells of the nucleus principalis propagated the information in its entirety, whereas the multi-whisker cells of the same nucleus and of the rostral nucleus interpolaris attenuated much of the low-frequency offset information. It is noteworthy that, although PrV predominantly projects to the lemniscal pathway via the thalamic ventral posteromedial nucleus (VPM)[32], its multi-whisker cells (PrVm) also contribute to the paralemniscal pathway through the thalamic posteromedial complex (POm)[33], which is the main target of SpVir[32]. Hence, both afferent sources to the paralemniscal pathway convey fast rhythmic information, whereas the afferent lemniscal pathway conveys information on both the fast and the slow components of whisking. This raises the possibility that one of the drives to the evolution of the lemniscal pathway[34] is to provide fast representation of object localization in head-related coordinates, by retaining both low- and high-frequency afferent information. These low- and high-frequency components can be compared downstream with their frequency-matched efference copies[35].

Our data indicate that the sensory organs of the vibrissal system extract information that is required for accurate interpretations of interactions with the environment without requiring copies of the efferent information from the motor system controlling the movement. These computations, which provide predictive information based on within-cycle accumulated information, are implemented by pre-neuronal computations dictated by the morphology and mechanics of the whisker-follicle complex. The contribution of this predictive encoding to the establishment of active vibrissal perception remains to be elucidated and will require future physiological and behavioral studies.

METHODS

Methods and any associated references are available in the online version of the paper.

Note: Any Supplementary Information and Source Data files are available in the online version of the paper.

ACKNOWLEDGMENTS

We thank D. Kleinfeld, N. Ulanovsky and A. Finkelstein for discussions. This research was supported by the Israel Science Foundation (grant no. 1127/14), the Minerva Foundation funded by the Federal German Ministry for Education and Research, the United States-Israel Binational Science Foundation (BSF, grant no. 2011432), the NSF-BSF Brain Research EAGER program (grant no. 2014906) and a fund from Lord Alliance for Life Science Collaboration. E.A. holds the Helen Diller Family Professorial Chair of Neurobiology.

AUTHOR CONTRIBUTIONS

A.W. and E.A. designed the experiments and the analyses. A.W. and K.B. performed the experiments. A.W. analyzed the data. All of the authors discussed the results and interpretations. A.W. wrote the manuscript. All of the authors discussed and commented on the manuscript.

COMPETING FINANCIAL INTERESTS

The authors declare no competing financial interests.

1. Ebara, S., Kumamoto, K., Matsuura, T., Mazurkiewicz, J.E. & Rice, F.L. Similarities and differences in the innervation of mystacial vibrissal follicle-sinus complexes in the rat and cat: a confocal microscopic study. *J. Comp. Neurol.* **449**, 103–119 (2002).
2. Maravall, M. & Diamond, M.E. Algorithms of whisker-mediated touch perception. *Curr. Opin. Neurobiol.* **25**, 176–186 (2014).
3. Kleinfeld, D. & Deschênes, M. Neuronal basis for object location in the vibrissa scanning sensorimotor system. *Neuron* **72**, 455–468 (2011).
4. Crochet, S. & Petersen, C.C. Correlating whisker behavior with membrane potential in barrel cortex of awake mice. *Nat. Neurosci.* **9**, 608–610 (2006).
5. Arkley, K., Grant, R.A., Mitchinson, B. & Prescott, T.J. Strategy change in vibrissal active sensing during rat locomotion. *Curr. Biol.* **24**, 1507–1512 (2014).
6. Sofroniew, N.J., Cohen, J.D., Lee, A.K. & Svoboda, K. Natural whisker-guided behavior by head-fixed mice in tactile virtual reality. *J. Neurosci.* **34**, 9537–9550 (2014).
7. Lenschow, C. & Brecht, M. Barrel cortex membrane potential dynamics in social touch. *Neuron* **85**, 718–725 (2015).
8. Szwed, M., Bagdasarian, K. & Ahissar, E. Encoding of vibrissal active touch. *Neuron* **40**, 621–630 (2003).
9. Ahissar, E. & Knutsen, P.M. Object localization with whiskers. *Biol. Cybern.* **98**, 449–458 (2008).
10. Curtis, J.C. & Kleinfeld, D. Phase-to-rate transformations encode touch in cortical eurons of a scanning sensorimotor system. *Nat. Neurosci.* **12**, 492–501 (2009).
11. Tonomura, S. *et al.* Structure-function correlations of rat trigeminal primary neurons: Emphasis on club-like endings, a vibrissal mechanoreceptor. *Proc. Jpn. Acad. Ser. B Phys. Biol. Sci.* **91**, 560–576 (2015).
12. Wolpert, D.M. & Kawato, M. Multiple paired forward and inverse models for motor control. *Neural Netw.* **11**, 1317–1329 (1998).
13. Hill, D.N., Curtis, J.C., Moore, J.D. & Kleinfeld, D. Primary motor cortex reports efferent control of vibrissa motion on multiple timescales. *Neuron* **72**, 344–356 (2011).
14. Deutsch, D., Pietr, M., Knutsen, P.M., Ahissar, E. & Schneidman, E. Fast feedback in active sensing: touch-induced changes to whisker-object interaction. *PLoS One* **7**, e44272 (2012).
15. Bale, M.R., Davies, K., Freeman, O.J., Ince, R.A. & Petersen, R.S. Low-dimensional sensory feature representation by trigeminal primary afferents. *J. Neurosci.* **33**, 12003–12012 (2013).
16. Sharpee, T., Rust, N.C. & Bialek, W. Analyzing neural responses to natural signals: maximally informative dimensions. *Neural Comput.* **16**, 223–250 (2004).
17. Quist, B.W., Seghete, V., Huet, L.A., Murphey, T.D. & Hartmann, M.J. Modeling forces and moments at the base of a rat vibrissa during noncontact whisking and whisking against an object. *J. Neurosci.* **34**, 9828–9844 (2014).
18. Yu, C. *et al.* Coding of object location in the vibrissal thalamocortical system. *Cereb. Cortex* **25**, 563–577 (2013).
19. Yu, C., Derdikman, D., Haidarliu, S. & Ahissar, E. Parallel thalamic pathways for whisking and touch signals in the rat. *PLoS Biol.* **4**, e124 (2006).
20. Mohar, B., Katz, Y. & Lampl, I. Opposite adaptive processing of stimulus intensity in two major nuclei of the somatosensory brainstem. *J. Neurosci.* **33**, 15394–15400 (2013).
21. Furuta, T. *et al.* Inhibitory gating of vibrissal inputs in the brainstem. *J. Neurosci.* **28**, 1789–1797 (2008).
22. Xiang, C., Arends, J.J. & Jacquin, M.F. Whisker-related circuitry in the trigeminal nucleus principalis: ultrastructure. *Somatosens. Mot. Res.* **31**, 141–151 (2014).
23. Knutsen, P.M., Biess, A. & Ahissar, E. Vibrissal kinematics in 3D: tight coupling of azimuth, elevation, and torsion across different whisking modes. *Neuron* **59**, 35–42 (2008).
24. Maravall, M., Alenda, A., Bale, M.R. & Petersen, R.S. Transformation of adaptation and gain rescaling along the whisker sensory pathway. *PLoS One* **8**, e82418 (2013).
25. Fairhall, A.L., Lewen, G.D., Bialek, W. & de Ruyter Van Steveninck, R.R. Efficiency and ambiguity in an adaptive neural code. *Nature* **412**, 787–792 (2001).
26. Seung, H.S. & Sompolinsky, H. Simple models for reading neuronal population codes. *Proc. Natl. Acad. Sci. USA* **90**, 10749–10753 (1993).
27. Knutsen, P.M., Pietr, M. & Ahissar, E. Haptic object localization in the vibrissal system: behavior and performance. *J. Neurosci.* **26**, 8451–8464 (2006).
28. Saraf-Sinik, I., Assa, E. & Ahissar, E. Motion makes sense: an adaptive motor-sensory strategy underlies the perception of object location in rats. *J. Neurosci.* **35**, 8777–8789 (2015).
29. Sanchez-Jimenez, A., Panetsos, F. & Murciano, A. Early frequency-dependent information processing and cortical control in the whisker pathway of the rat: electrophysiological study of brainstem nuclei principalis and interpolaris. *Neuroscience* **160**, 212–226 (2009).
30. Sreenivasan, V., Karmakar, K., Rijli, F.M. & Petersen, C.C. Parallel pathways from motor and somatosensory cortex for controlling whisker movements in mice. *Eur. J. Neurosci.* **41**, 354–367 (2014).
31. Timofeeva, E., Dufresne, C., Sík, A., Zhang, Z.W. & Deschênes, M. Cholinergic modulation of vibrissal receptive fields in trigeminal nuclei. *J. Neurosci.* **25**, 9135–9143 (2005).
32. Deschenes, M. & Urbain, N. Vibrissal afferents from trigeminus to cortices. *Scholarpedia* **4**, 7454 (2009).
33. Veinante, P. & Deschênes, M. Single- and multi-whisker channels in the ascending projections from the principal trigeminal nucleus in the rat. *J. Neurosci.* **19**, 5085–5095 (1999).
34. Bishop, G.H. The relation between nerve fiber size and sensory modality: phylogenetic implications of the afferent innervation of cortex. *J. Nerv. Ment. Dis.* **128**, 89–114 (1959).
35. Fee, M.S., Mitra, P.P. & Kleinfeld, D. Central versus peripheral determinants of patterned spike activity in rat vibrissa cortex during whisking. *J. Neurophysiol.* **78**, 1144–1149 (1997).

ONLINE METHODS

Surgical procedures. Experiments were performed on 15 male albino Wistar rats (250–350 g). Animal maintenance, manipulations, procedures, and surgeries were conducted in accordance with the National Institutes of Health Guide for the Care and Use of Laboratory Animals and were approved by the Institutional Animal Care and Use Committee of The Weizmann Institute. Surgical procedures were performed under general anesthesia as described previously[8,19,36]. In brief, rats were anesthetized to surgical levels using intraperitoneal injections of urethane (1.5 g per kg of body weight), placed on a regulated heating pad, and maintained when required with supplemental injections of urethane (10% of the initial dose). Atropine methyl nitrate (0.3 mg per kg, intramuscular) was administered to prevent respiratory complications. Anesthetized animals were mounted in a stereotaxic device (SR-6; Narishige; Japan). Body temperature was maintained at 37 °C during the experiment. The left buccal branch[37] of the facial nerve was exposed and isolated at the middle cheek level, and mounted on a pair of silver hook electrodes for stimulation. Ipsilateral craniotomy was performed over the left trigeminal ganglion or the left trigeminal nuclei (SpVir, PrV) of the brainstem according to stereotaxic coordinates[38,39].

Electrophysiology. During each recording, up to four tungsten microelectrodes (0.8–1.2 MΩ, Alpha Omega Engineering) were lowered in parallel until units drivable by manual whisker stimulations were encountered at the appropriate stereotaxic depth. To determine the receptive fields (RFs) of the recording units, single units were sorted online (ALAB-ASD3.1, Alpha-Omega Engineering), and the whiskers that evoked a noticeable response to a manual passive deflection were noted. While performing our closed-loop stimulation, extracellular voltage was sampled at 50 kHz (MCP PLUS, Alpha-Omega Engineering). Single units were sorted offline by performing principal component and clustering analyses. Units were considered to be 'single', that is, to represent individual neurons, only if their spike shapes were homogenous, and did not overlap with other units or noise, and if the units exhibited refractory periods of >1 ms in autocorrelation histograms. The RFs that were measured online were assigned to offline sorted units by matching spike shapes. The artifacts produced by electrical stimulation were identified in the clustering analysis and completely removed from analysis. In total, 194 single units were recorded, out of which 147 fired more than 50 spikes and were analyzed here: 47 units in the TG of 5 different rats; 34 units in the PrV (9 with single-whisker RF and 25 with multi-whisker RF) of 4 different rats; 14 additional PrV units with unknown RFs were not included in our analyses; and 52 units in the SpVir of 6 different rats.

Experimental setup. Management of the experimental setup (extracellular and video recordings, whisker tracking, closed-loop control algorithm and delivery of stimulation) was performed using a custom made real-time application (Labview, National Instruments).

Whisker tracking. Whisker movements were recorded at 500 frames per s with a fast digital video camera (Basler 504k, Basler). Video recordings were synchronized with neurophysiological data with 1-ms accuracy[8]. Whisker motion was tracked online: the two most dorsal rows (A and B) were trimmed to 5-mm length; a small (~1 cm) section of three whiskers in the third row (C1-C3), closest to the skin, was lightly stained with black eye-liner to improve contrast; these three whisker sections were detected in real time on a frame-by-frame basis and fitted with a quadratic polynomial. Protraction angles, curvatures at base and follicle translations for each tracked whisker were extracted from these polynomials[40]. All experiments involved artificial whisking in free air[8,19,36], and so protractions of all whiskers were highly correlated and changes in curvatures were negligible. We therefore chose the protraction angle of the middle whisker C2, relative to its angle at rest, as the main whisker state variable θ.

Closed-loop control and stimulation. Biphasic, rectangular electrical pulses (15–50-µs duration) were generated and delivered to the facial nerve every 12 ms using a digital-to-analog converter (NI PCI-6221, National Instruments). The amplitude of each pulse (0–1.5 V, 1-mV resolution) was controlled online using a commonly-used motion control algorithm, which consists of a feed-forward inverse model and a feedback proportional-integral (PI) controller[41]. The inverse model was realized using a standard artificial neural network with a single, three-neuron hidden layer. This network was iteratively trained using the back-propagation algorithm at the beginning of each experiment. The PI controller counteracted slow drifts and changes in the motor plant's response, thus converging the tracked whisking protraction angle θ toward a pre-defined desired whisking trajectory θ^*. Two protocols were used to define this desired trajectory: synthetic whisking and awake playback. In synthetic whisking, a long whisking sequence (1,000 cycles, divided into 20–50 bouts separated by 2–5-s rest intervals) was synthesized artificially using the rhythmic decomposition model[13]: $\theta^*(t) = \theta_{amp}(t)\ cos(\varphi(t)) + \theta_{off}(t)$, where φ is the whisking phase (oscillates from $-\pi$ to π with frequency f) and θ_{amp} and θ_{off} are the slowly varying whisking amplitude the offset. These parameters were randomly generated within the behaviorally relevant and technically constrained bounds ($0\leq \theta_{amp} \leq 18$; $0\leq \theta_{off} \leq 35$; $4\leq f \leq 10$). Note that, while θ_{amp} and θ_{off} were changed slowly (3–5-cycle-long correlations), f was randomized for each cycle independently (see **Supplementary Fig. 2**). In awake playback, an 8.5-s-long whisking trajectory was extracted from a video recording of an awake, freely exploring rat. The trajectory chosen contained 'open-air' whisking only, that is the whiskers did not contact any object during these 8.5 s. In each recording, this trajectory was presented 18 times with 2–5-s rest intervals. The first repetition was removed from analysis to exclude control algorithm convergence and neuronal transients. In open-loop stimulation (**Supplementary Fig. 4**), 8-Hz rectangular pulse trains with duty-cycle 50% were applied[8] at various voltage amplitudes (600–2,000 mV), given at random. This was applied on 22 of recorded TG cells.

Histology. At the end of each recording session in the brainstem nuclei under study, electrolytic lesions were induced by passing currents (50–100 µA, 4 s, unipolar) through the tips of the recording electrodes. At the end of each experiment the rat brain was removed, fixed, sliced parasagittally and stained for cytochrome oxidase[14,22]. Using this technique, lesions located in the nuclei under the study were clearly seen. Only neurons for which the recording site was clearly located were included in this study (see **Supplementary Fig. 6** for examples). In recording sessions from trigeminal ganglion histological procedures were not conducted, since the anatomic location of the ganglion and the highly typical responses of the primary afferent cells precluded another source of recordings[8,38,43].

Analysis. *Tuning maps.* The range of each variable of interest (for example, angle θ, phase φ, etc.) was divided into 24 bins. The conditional firing probability with relation to variable (or set of variables) s, denoted $p(r|s)$, was computed by dividing the spike occurrence histogram (that is, the number of samples within each bin in which a spike occurred) with the sample occurrence histogram (that is, the total number of samples within each bin). All two-dimensional maps (for example, $p(r\,|\,\theta,\dot{\theta})$) are presented as images with probability scaled to the range [0,1] and linearly color coded (blue = 0 and red = 1). Bins in which the sample occurrence was smaller than 20 were removed from analysis and are colored white.

STA and MID. The STA characterizes the projection within the input space (in our case, the whisking kinematic space) most correlated with spikes generated by a neuron[2,15]. While being easy to compute and interpret, the STA was shown to be heavily biased by input statistics and as such it is less applicable for natural inputs[16]. An alternative, more suitable projection is the MID, which indicates the direction in input space yielding the highest mutual information with spiking activity[16]. It is found iteratively by using an algorithm that combines gradient ascent and simulated annealing. For each neuron, this algorithm was repeated ten times with different starting points, to rule-out convergence to local minima. Two MID projections were computed for each neuron: a non-causal projection (that is, using past and future dynamics; **Fig. 2a**) for the purpose of extracting the preferred phase within a cycle, and a causal projection (that is, using only past dynamics) for the purpose of modeling (see below and **Supplementary Fig. 3**).

Preferred phase and phase selectivity. The tuning of each unit to phase, $p(r|\varphi)$, was summed in the complex plane to produce the unit's phase vector:

$$p_\varphi = \sum_{\varphi i=-\pi}^{\pi} p(r\,|\,\varphi_i)e^{i\varphi_i}$$

Therefore, the preferred phase of the unit is the argument (angle) of the phase vector, $\tilde{\varphi} = \mathrm{Arg}(p_\varphi)$, while the phase selectivity is the length of the vector, $S = |p_\varphi|$ (see **Supplementary Fig. 3** for examples).

Frequency and amplitude invariance. To measure the invariance of the phase tuning to frequency/amplitude, the preferred phase was computed

doi:10.1038/nn.4221

separately for high (above median) and low (below median) frequency/amplitude. The frequency/amplitude invariance index (FII/AII) was defined to be the difference (in radians) between the high and low preferred phases. To assess the statistical significance of the frequency- and amplitude-invariance of the preferred phase, we employed a Monte-Carlo approach: (i) the phase-tuning of each cell ($p(r|\varphi)$) was used to produce spike-rate dynamics from the recorded phase dynamics; (ii) 5,000 non-homogenous Poisson spike trains were generated using the obtained spike-rate. These spike trains have the overall phase tuning of the cell but are frequency- and amplitude-invariant by construct; (iii) the FII and AII were calculated for each spike train; (iv) the significance of frequency/amplitude dependence of the cell's preferred phase was determined as the percentage of simulated FII/AIIs that were smaller (in their absolute value) than the FII/AII of the cell. The preferred phase was deemed invariant if this percentage was greater or equal to 0.05. The same procedure was used to assess the invariance of the models' preferred phase.

Information content. To determine the information the spiking response r contains on variable (or set of variables) s, the normalized mutual information was estimated:

$$U(r\,|\,s) = \frac{I(r,s)}{H(r)} = 1 - \frac{H(r\,|\,s)}{H(r)}$$

where I is the mutual information and H is the information entropy. The conditional entropy was calculated using the conditional probability functions (tuning maps) estimated as described above. Note that $0 \le U(r|s) \le 1$, with $U(r|s) = 0$ when the spiking is completely independent of the variable s, and $U(r|s) = 1$ when the firing is completely predictable given the variable s.

Rhythmicity index. The rhythmicity index for each unit is defined as $RI = U(r|\varphi,\theta_{amp})/U(r|\theta_{off})$, namely the ratio between the information conveyed about the high-frequency, rhythmic component and the information conveyed about the low-frequency, offset component of whisking.

Population rate analysis. Only neurons that fired at least one spike in the 'awake playback' protocol were included ($n = 102$). To quantify population sensitivity to the different frequencies, the firing rate of each population was computed using 14-ms bins and then filtered to the low (<4 Hz) and high (>4 Hz) frequency bands (yielding r_{LPF} and r_{HPF}, respectively). Likewise, whisker motion was decomposed to low-frequency offset (θ_{off}) and high frequency oscillations. The normalized cross-correlation between activity and movement was calculated for each frequency band and the peak value, C_{max}, was extracted.

Statistics. The bootstrap method was in all comparisons between populations (5,000 random draws of the data). Random permutations were used to evaluate significance of correlations (10^4 random permutations). Wilcoxon signed-rank test was used to measure invariance (divergence of median from zero). Pearson's chi-square test was used to check overrepresentation of protraction phases (divergence from uniform distribution). These tests were chosen due to the relatively few underlying assumptions (independence of samples). To determine whether the information the firing of a unit contains on a certain variable s is statistically significant, we employed a Monte-Carlo approach: (i) the information content of the variable, $U(r|s)$ was calculated; (ii) 500 random spike-trains r_i were generated with the same number of spikes as the recorded unit emitted; (iii) for each control spike-train the information content $U(r_i|s)$ was calculated; (iv) The information is considered significant if $U(r|s) \ge U(r_i|s)$ for > 95% of r_i's. Of all 147 analyzed units, 10 had no significant information on any whisking variable. Sample sizes were determined by statistical requirements, aiming at confidence levels >95%. No statistical methods were used to predetermine sample sizes but our sample sizes are similar to those generally employed in the field. No randomization or blinding was used is this study.

Simulations. *LNP model.* A causal MID filter (in a 100-ms time window) was computed from the spike-train of each unit[16]. The units' tuning to this MID projection $p(r|MID)$ was also computed. To check the capacity of linear filtering to extract phase information, a Linear-Nonlinear-Poisson model[44] was constructed for each unit, with the causal MID filter as the linear stage and the tuning $p(r|MID)$ as the nonlinear stage. The model was then driven by the same whisking sequence presented to the original unit. The output of the nonlinear stage served as a rate function for a non-homogeneous Poisson process. Ten spike trains were randomly generated from this rate function and the phase tuning was analyzed for each. Finally, the results were averaged over the ten repetitions (**Supplementary Fig. 3**).

Kinematic model. For each cell, half of the synthetic whisking data was used to compute the first-order kinematic response (**Fig. 2a**), which was then fitted with a bivariate Gaussian

$$P(r\,|\,\theta,\dot{\theta}) \cong \frac{a}{2\pi\sigma_\theta\sigma_{\dot{\theta}}\sqrt{1-\rho^2}}\, e^{-\frac{2}{1-\rho^2}\left(\frac{(\theta-\mu_\theta)^2}{\sigma_\theta^2}+\frac{(\dot{\theta}-\mu_{\dot{\theta}})^2}{\sigma_{\dot{\theta}}^2}-\frac{2\rho(\theta-\mu_\theta)(\dot{\theta}-\mu_{\dot{\theta}})}{\sigma_\theta\sigma_{\dot{\theta}}}\right)}$$

where a is the response intensity, $(\mu_\theta,\mu_{\dot{\theta}})$is the location of the peak, σ_θ and $\sigma_{\dot{\theta}}$ the width in each coordinate and ρ the obliqueness. The kinematics of the second half of the data was then converted using the fitted Gaussian to the rate function of a non-homogeneous Poisson process. Ten spike trains were randomly generated from this rate function and the phase tuning was analyzed for each. Finally, the results were averaged over the ten repetitions (**Supplementary Fig. 3**).

Brainstem post-synaptic current model. Simulations were used to test the hypothesis that short term synaptic depression underlies offset filtering. Each spike, from any of the TG cells recorded, contributed an exponentially decaying excitatory post-synaptic current (EPSC, $\tau_{EPSC} = 10$ ms). The synaptic efficacies w_k, determining the amplitude of each EPSC, followed classic STD dynamics[45]: $w_k(t_{sp}^+) = (1 - D)w_k(t_{sp}^-)$; $\tau_{STD}\dot{w}_k = 1 - w_k$, where t_{sp} are the spike times, D the resource utilization coefficient and $\tau_{STD} = 200$ms is the synaptic recovery time constant. D was varied from 0 (no STD) to 0.2 (strong STD). EPSCs from all driving TG cells were summed to produce the total post-synaptic membrane current I. To check the effect of presynaptic population size, the number of TG cells used was altered between one and 32. 50 random collections of TG cells were taken for each size ($D = 0.2$). To check the robustness of the model to changes in parameters, τ_{STD} and τ_{EPSC} were altered in the range 50–300 ms and 5–25 ms, respectively. Note that τ_{EPSC} in this model represents both the synaptic and membrane time constants.

A **Supplementary Methods Checklist** is available.

36. Derdikman, D. *et al.* Layer-specific touch-dependent facilitation and depression in the somatosensory cortex during active whisking. *J. Neurosci.* **26**, 9538–9547 (2006).
37. Semba, K. & Egger, M.D. The facial "motor" nerve of the rat: control of vibrissal movement and examination of motor and sensory components. *J. Comp. Neurol.* **247**, 144–158 (1986).
38. Shoykhet, M., Doherty, D. & Simons, D.J. Coding of deflection velocity and amplitude by whisker primary afferent neurons: implications for higher level processing. *Somatosens. Mot. Res.* **17**, 171–180 (2000).
39. Paxinos, G. & Watson, C. *The Rat Brain in Stereotaxic Coordinates*, 4th edn (Academic Press, 1998).
40. Bagdasarian, K. *et al.* Pre-neuronal morphological processing of object location by individual whiskers. *Nat. Neurosci.* **16**, 622–631 (2013).
41. Kawato, M. Internal models for motor control and trajectory planning. *Curr. Opin. Neurobiol.* **9**, 718–727 (1999).
42. Haidarliu, S. & Ahissar, E. Spatial organization of facial vibrissae and cortical barrels in the guinea pig and golden hamster. *J. Comp. Neurol.* **385**, 515–527 (1997).
43. Zucker, E. & Welker, W.I. Coding of somatic sensory input by vibrissae neurons in the rat's trigeminal ganglion. *Brain Res.* **12**, 138–156 (1969).
44. Chichilnisky, E.J. A simple white noise analysis of neuronal light responses. *Network* **12**, 199–213 (2001).
45. Tsodyks, M.V. & Markram, H. The neural code between neocortical pyramidal neurons depends on neurotransmitter release probability. *Proc. Natl. Acad. Sci. USA* **94**, 719–723 (1997).